SCIENTIFIC REPORTS

OPEN

SUBJECT AREAS:
CHEMOTHERAPY
CALCIUM SIGNALLING

Received
5 November 2013

Accepted
20 May 2014

Published
5 June 2014

Correspondence and requests for materials should be addressed to H.-J.C. (hjchae@chonbuk.ac.kr)

Bax Inhibitor-1-Mediated Inhibition of Mitochondrial Ca^{2+} Intake Regulates Mitochondrial Permeability Transition Pore Opening and Cell Death

Geum-Hwa Lee[1], Hwa-Young Lee[1], Bo Li[1], Hyung-Ryong Kim[2] & Han-Jung Chae[1]

[1]Department of Pharmacology and Cardiovascular Research Institute, Medical School, Chonbuk National University, Jeonju, 561-181, Republic of Korea, [2]Department of Dental Pharmacology and Wonkwang Dental Research Institute, School of Dentistry, Wonkwang University, Iksan, 570-749, Republic of Korea.

A recently studied endoplasmic reticulum (ER) stress regulator, Bax inhibitor-1 (BI-1) plays a regulatory role in mitochondrial Ca^{2+} levels. In this study, we identified ER-resident and mitochondria-associated ER membrane (MAM)-resident populations of BI-1. ER stress increased mitochondrial Ca^{2+} to a lesser extent in BI-1–overexpressing cells (HT1080/BI-1) than in control cells, most likely as a result of impaired mitochondrial Ca^{2+} intake ability and lower basal levels of intra-ER Ca^{2+}. Moreover, opening of the Ca^{2+}-induced mitochondrial permeability transition pore (PTP) and cytochrome c release were regulated by BI-1. In HT1080/BI-1, the basal mitochondrial membrane potential was low and also resistant to Ca^{2+} compared with control cells. The activity of the mitochondrial membrane potential-dependent mitochondrial Ca^{2+} intake pore, the Ca^{2+} uniporter, was reduced in the presence of BI-1. This study also showed that instead of Ca^{2+}, other cations including K^+ enter the mitochondria of HT1080/BI-1 through mitochondrial Ca^{2+}-dependent ion channels, providing a possible mechanism by which mitochondrial Ca^{2+} intake is reduced, leading to cell protection. We propose a model in which BI-1–mediated sequential regulation of the mitochondrial Ca^{2+} uniporter and Ca^{2+}-dependent K^+ channel opening inhibits mitochondrial Ca^{2+} intake, thereby inhibiting PTP function and leading to cell protection.

The endoplasmic reticulum (ER) contains a high concentration of Ca^{2+} in the millimolar range[1,2]; other organelles, such as mitochondria, also contain Ca^{2+}, but only in the micromolar range[3]. In normal or adaptive conditions, Ca^{2+} is released from the ER and transferred to the mitochondria, in which the fine modulation of Ca^{2+} homeostasis plays a fundamental role in normal mitochondria physiology[4,5]. However, abnormal Ca^{2+} efflux from the ER and Ca^{2+} accumulation in the mitochondria are linked to the effects of apoptotic stimuli, including ER stress[6]. In addition, mitochondrial Ca^{2+} levels and opening of the mitochondrial membrane permeability transition pore (PTP) have recently been proposed to play a role in ER stress-induced cell death[7].

Bax inhibitor-1 (BI-1) performs a protective role against ER stress-induced cell death[8–10]. Embryonic fibroblasts from BI-$1^{-/-}$ mice are hypersensitive to ER stress-induced apoptosis, a finding that has been attributed to increased release of Ca^{2+} from the internal stores[8]. Recently, BI-1-mediated protection against ER stress was proposed to be involved in Ca^{2+} regulation[11], implying that BI-1 may possess a pH-sensitive motif for sensing cellular pH. The low levels of $[Ca^{2+}]_{ER}$ observed upon overexpression of BI-1 are related to a low mitochondrial Ca^{2+} concentration ($[Ca^{2+}]_{mito}$) in BI-1-overexpressing cells[12]. Considering that the mechanism of ER stress-induced cell death involves both the ER and mitochondria[13], low $[Ca^{2+}]_{ER}$ in HT1080/BI-1 may affect $[Ca^{2+}]_{mito}$, which likely plays a role in cell protection. However, $[Ca^{2+}]_{mito}$ can be also affected by mitochondrial physiological functions[14]. For example, the mitochondrial membrane potential ($\Delta\psi m$) is both directly and indirectly related to mitochondrial Ca^{2+} channel-like proteins, such as the Ca^{2+} uniporter[15] and the Ca^{2+}-dependent mitochondrial K^+ channel[16].

The role of BI-1 has been also studied in the context of mitochondrial physiology. A recent study using a yeast system to investigate the effects of *Arabidopsis* BI-1 (AtBI-1) concluded that mitochondrial electron transport chain proteins are required for BI-1-mediated protection against Bax[17]. Overexpression of BI-1 has also been

shown to alter mitochondrial function through a mechanism proposed to involve reduced mitochondrial glucose metabolism and O_2 consumption[18]. Although the extent to which BI-1 affects various parameters of mitochondrial function, such as $\Delta\psi m$, has not been fully clarified, we hypothesize that BI-1 affects $[Ca^{2+}]_{mito}$, thereby altering mitochondrial function. In this study, we focused on elucidating the mechanism by which BI-1 reduces $[Ca^{2+}]_{mito}$ by examining the opening of the mitochondrial permeability transition pore and the subsequent release of cytochrome c. We also investigated the relationship between $[Ca^{2+}]_{mito}$ and the regulation of cell death by BI-1.

Results

BI-1 is localized to mitochondria-associated membranes and the ER. To gain insight into the role of BI-1 in mitochondrial function, we first determined its subcellular localization. Initially, we performed biochemical fractionation of HT1080 fibrosarcoma cells stably transfected with either a construct conferring neomycin resistance (HT1080/Neo), or a construct driving the overexpression of BI-1 (HT1080/BI-1). Western blot analysis of the fractions revealed that some of the BI-1 was fractionated with the mitochondria-associated membrane (MAM), although the majority was fractionated with the ER (Fig. 1A). Expression of BI-1 was also observed in crude mitochondria fractions but not in pure mitochondria fractions, showing the absence of BI-1 in the mitochondria organelle.

We also confirmed the integrity of each fraction by immunoblotting for subcellular organelle marker proteins: calnexin for ER and MAM, Tom20 for mitochondria, and voltage-dependent anion channel (VDAC) which enrich in pure mitochondria and also present in MAM[3,19–21] (Fig. 1A). In addition, we performed ultrastructural studies to analyze the localization of BI-1. Electron microscopy (EM) images of HA-immunogold staining revealed that the majority of BI-1 was ER-localized and a detectable proportion was also present on the MAM (Fig. 1B). Similarly, in a fluorescence study, BI-1 expression was co-localized with calnexin and VDAC (Fig. 1C). Figure 1D shows quantitative analysis of the overlap between BI-1 and calnexin (about 55%) or between BI-1 and VDAC (about 20%). Consistent with previous findings, these data indicated that BI-1 protein was clearly observed in MAM, as well as the ER.

BI-1 regulates ER stress-induced mitochondrial Ca^{2+} accumulation. The protective role of BI-1 against ER stress-induced cell death has been well characterized[8,10,22]. Because the accumulation of mitochondrial Ca^{2+} plays a role in ER stress-induced cell death[23], we investigated the effect of BI-1 on $[Ca^{2+}]_{mito}$. We measured thapsigargin-stimulated $[Ca^{2+}]_{mito}$ using the fluorescent dye Rhod II, and observed that HT1080/BI-1 exhibited lower levels of fluorescence than parental HT1080 cells or control, HT1080/Neo (Fig. 2A). Next, we analyzed thapsigargin-induced $[Ca^{2+}]_{ER}$ changes in the absence of extracellular Ca^{2+} using an ER-targeted version of aequorin (erAEQ). Even in the absence of ER stress,

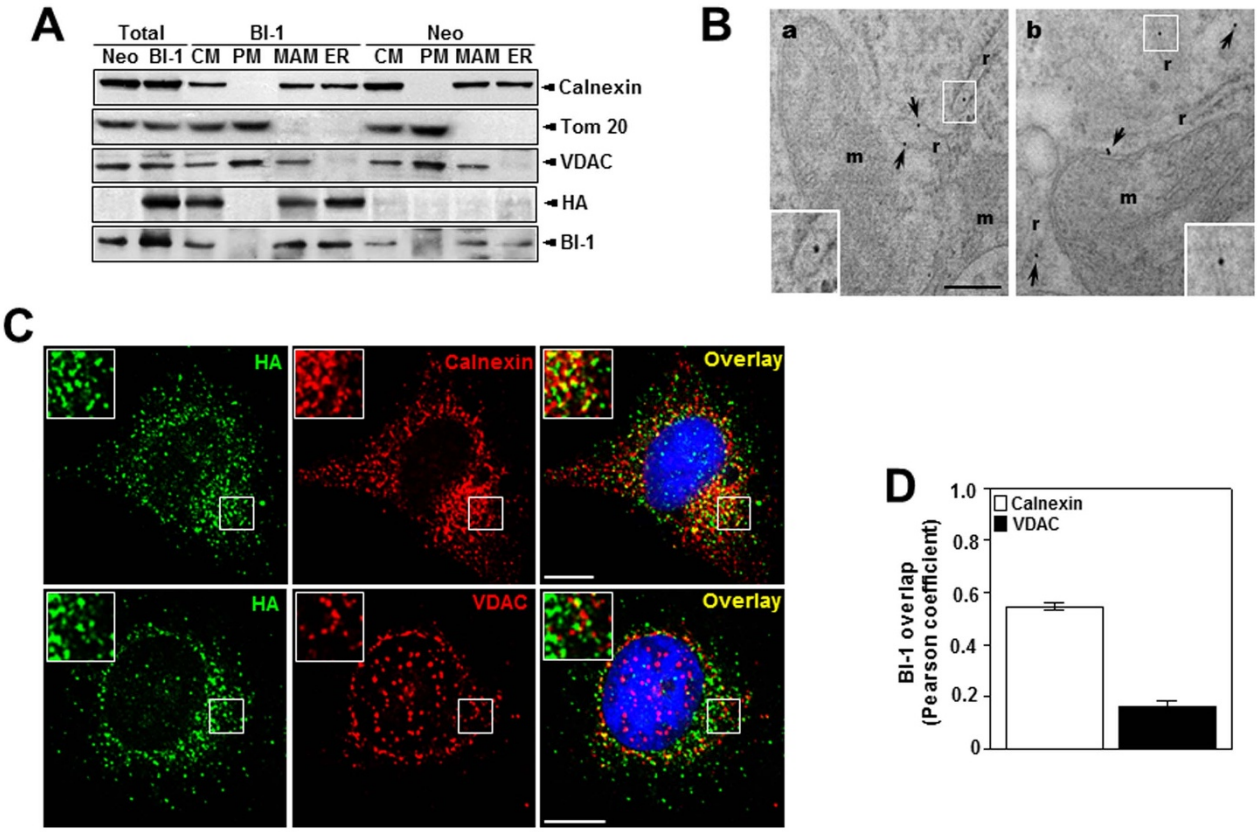

Figure 1 | BI-1 localizes to mitochondria and the ER. (A) After subcellular fractionation of HT1080/BI-1cell lysates, immunoblotting was performed with antibodies against calnexin, Tom20, VDAC, HA, and BI-1. (B) Electron microscopy analysis of BI-1 localization. Immunogold labeling of HA-BI-1 was performed as described in Materials and Methods. The right panel shows anti-rat HA antibody and the left panel shows anti-mouse HA antibody. Arrows indicate BI-1-positive ER or MAM regions. (C) Confocal laser scanning microscope images of HT1080/BI-1. HT1080/BI-1 cells were fixed, permeabilized, and immunostained with anti-HA, anti-calnexin (upper panel), or anti-VDAC (lower panel) antibodies prior to imaging on a confocal laser scanning microscope. (D) Quantification of BI-1–calnexin and BI-1–VDAC co-localization was performed. Cropped gels/blots were run under the same experimental conditions. M, mitochondria; ER, endoplasmic reticulum; CM, crude mitochondria; PM, pure mitochondria; MAM, mitochondria-associated membrane; Neo, neomycin-resistant pcDNA3-transfected HT1080 cells (HT1080/Neo); BI-1, HA-BI-1-pcDNA3-transfected HT1080 cells (HT1080/BI-1).

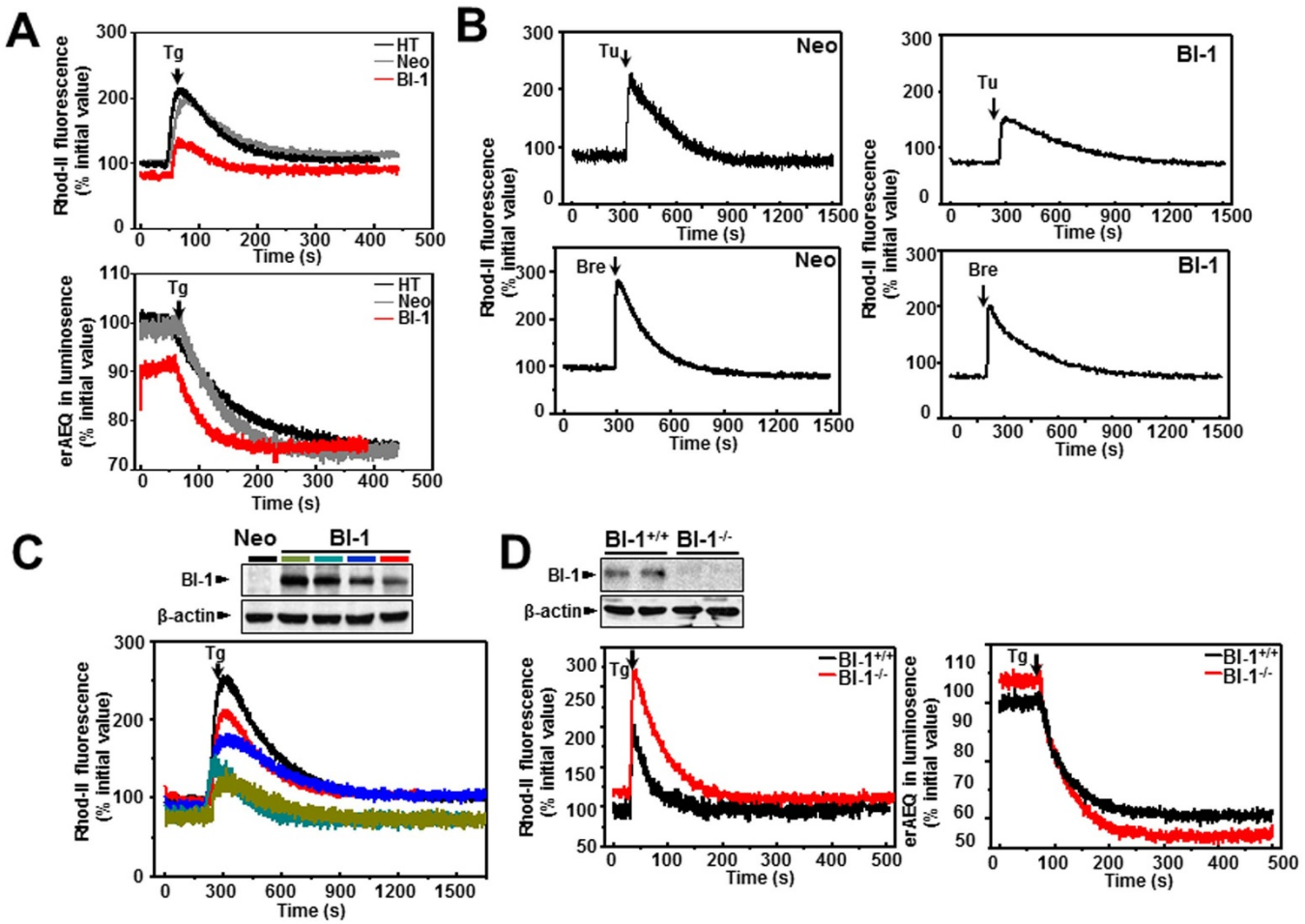

Figure 2 | Low $[Ca^{2+}]_{ER}$ leads to low $[Ca^{2+}]_{mito}$ in HT1080/BI-1 cells. (A) Mitochondrial and ER Ca^{2+} in parental HT1080, HT1080/Neo, and HT1080/BI-1 cells after treatment with 5 μM thapsigargin (arrow) was analyzed with Rhod II AM fluorescence (upper) and erAEQ luminescence (lower), respectively. (B) HT1080/Neo and HT1080/BI-1 were loaded with Rhod II AM and treated with either 5 μg/ml tunicamycin or 1 μg/ml brefeldin A (arrow). Rhod II fluorescence was monitored over time. (C) Immunoblotting of HT1080/Neo and HT1080 cells expressing different amounts of BI-1 with antibodies against BI-1 and β-actin (upper). Mitochondrial Ca^{2+} in HT1080/Neo and BI-1–expressing HT1080 cells upon treatment with 5 μM thapsigargin was analyzed by Rhod II AM fluorescence. Specific colors indicate cells expressing different amounts of BI-1. (D) Immunoblotting of BI-$1^{+/+}$ and BI-$1^{-/-}$ MEF cells with antibodies against BI-1 and β-actin (upper). BI-$1^{+/+}$ and BI-$1^{-/-}$ MEF cells were incubated with Rhod II AM to analyze mitochondrial accumulation of Ca^{2+} after treatment with 5 μM thapsigargin (arrow) (left). BI-$1^{+/+}$ and BI-$1^{-/-}$ MEF cells were transfected with erAEQ. The intensity of erAEQ luminescence was monitored after treatment with 5 μM thapsigargin (arrow) (right). Results represent the mean ± SEM of five independent experiments. Tg, thapsigargin; Tu, tunicamycin; Bre, Brefeldin A; erAEQ, ER-localized aequorin; HT, parental HT1080 cells; Neo, neomycin-resistant pcDNA3-transfected HT1080 cells (HT1080/Neo); BI-1, HA-BI-1-pcDNA3-transfected HT1080 cells (HT1080/BI-1).

HT1080/BI-1 showed lower levels of erAEQ luminescence than parental HT1080 or HT1080/Neo cells (Fig. 2A, lower), indicating that HT1080/BI-1 cells have lower $[Ca^{2+}]_{ER}$. We next exposed cells to classic ER stress-inducing agents, such as tunicamycin, an inhibitor of N-acetylglycosylation, and brefeldin A, a protein transport inhibitor (Fig. 2B). Both agents markedly increased $[Ca^{2+}]_{mito}$; however, HT1080/BI-1 exhibited lower $[Ca^{2+}]_{mito}$ than HT1080/Neo. The basal $[Ca^{2+}]_{mito}$ was also consistently lower in HT1080/BI-1 than in HT1080/Neo. To further clarify the protective role of BI-1 against mitochondrial Ca^{2+}, we developed cell lines with different levels of BI-1 expression. Thapsigargin-induced mitochondrial Ca^{2+} was regulated in a BI-1 expression-dependent manner (Fig. 2C). Furthermore, the decrease in $[Ca^{2+}]_{ER}$ and the increase in $[Ca^{2+}]_{mito}$ were consistently of a higher magnitude in BI-1 knockout mouse embryonic fibroblasts (BI-$1^{-/-}$ MEF cells) compared with BI-1 wild-type cells (BI-$1^{+/+}$) (Fig. 2D).

Mitochondrial Ca^{2+} intake is reduced in HT1080/BI-1 cells. To confirm the low mitochondrial Ca^{2+} in the HT1080/BI-1, we indirectly measured $[Ca^{2+}]_{mito}$ in Fura-2AM-loaded HT1080/Neo and HT1080/BI-1. As expected, the increase in intracellular Ca^{2+} ($[Ca^{2+}]_i$) was significantly lower in HT1080/BI-1, compared with HT1080/Neo, upon treatment with a mitochondrial uncoupler, carbonylcyanide m-chlorophenylhydrazone (CCCP) (Fig. 3A). This suggests that the $[Ca^{2+}]_{mito}$ was lower in the BI-1 overexpressing system compared with the control. Analysis of Rhod II fluorescence revealed that HT1080/BI-1 accumulated less mitochondrial Ca^{2+} than HT1080/Neo (Fig. 3B), consistent with the results shown in Figure 3A. We next examined $^{45}Ca^{2+}$ intake by mitochondrial membrane fractions and found that $^{45}Ca^{2+}$ intake by mitochondria from HT1080/BI-1 was significantly lower than that by mitochondria from HT1080/Neo (Fig. 3C). Direct exposure of mitochondria to Ca^{2+} also revealed lower levels of mitochondrial Ca^{2+} intake in HT1080/BI-1 compared with HT1080/Neo (Fig. 3D).

The Ca^{2+} uniporter is involved in mitochondrial Ca^{2+} intake in HT1080/BI-1 cells. To further investigate the mechanism underlying the reduced $[Ca^{2+}]_{mito}$ intake in HT1080/BI-1, we examined

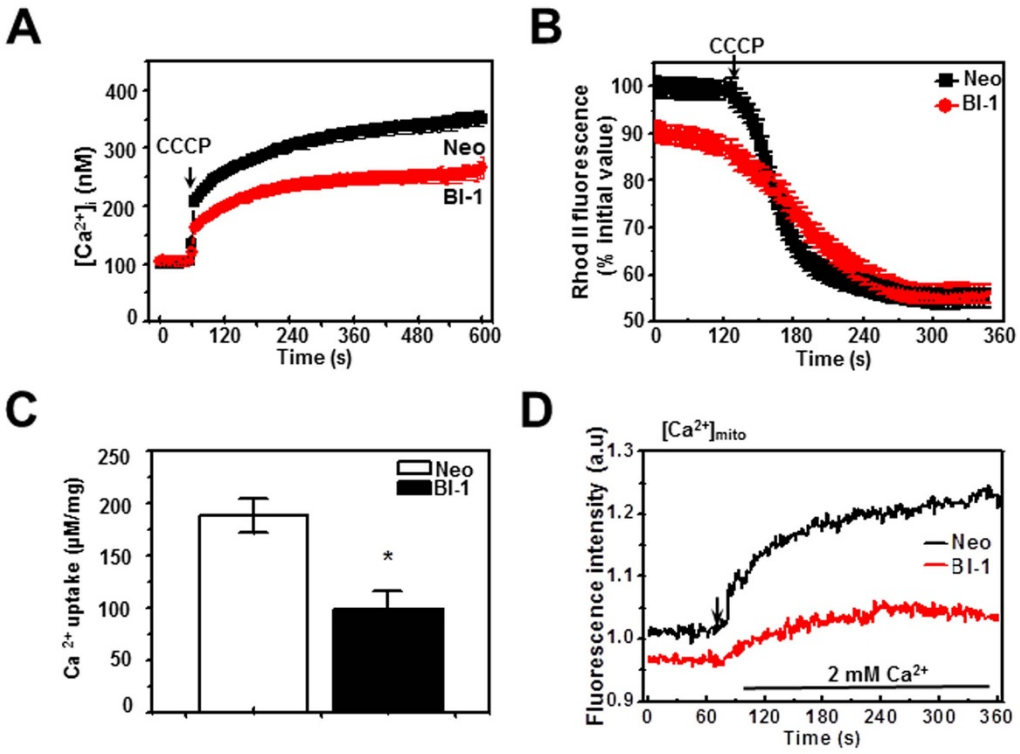

Figure 3 | HT1080/BI-1 cells exhibit reduced levels of mitochondrial Ca^{2+} compared with control cells. (A) HT1080/Neo and HT1080/BI-1 cells were loaded with Fura2-AM and subsequently exposed to the mitochondrial inhibitor CCCP (1 μM). Representative Ca^{2+} traces are shown. Individual cells were imaged (n = 20) and their fluorescence intensities (Fura2) recorded; the peaks of Ca^{2+} release are also shown. (B) HT1080/Neo and HT1080/BI-1 cells were loaded with Rhod II AM and subsequently treated with CCCP (1 μM). Rhod II fluorescence was monitored in individual cells (n = 15). (C) Mitochondria were analyzed for $^{45}Ca^{2+}$ intake. *, $p < 0.05$ versus HT1080/Neo. (D) Mitochondria from HT1080/Neo and HT1080/BI-1 were loaded with Rhod II AM and subsequently treated with 2 mM $CaCl_2$. Rhod II fluorescence was monitored. $[Ca^{2+}]_i$, intracellular Ca^{2+}; Tg, thapsigargin; CCCP, carbonylcyanide m-chlorophenylhydrazone; Neo, neomycin-resistant pcDNA3-transfected HT1080 cells (HT1080/Neo); BI-1, HA-BI-1-pcDNA3-transfected HT1080 cells (HT1080/BI-1).

whether the Ca^{2+} uniporter is involved. This channel regulates both $[Ca^{2+}]_{mito}$ intake and ER stress-induced cell death[23]. Using the Rhod II fluorescence assay, we observed that RU360-mediated inhibition of the Ca^{2+} uniporter decreased $[Ca^{2+}]_{mito}$ intake in HT1080/Neo, but had a smaller effect in HT1080/BI-1 (Fig. 4A). The values of $[Ca^{2+}]_{ER}$ and $[Ca^{2+}]_{mito}$ with or without RU360 treatment were shown in Fig. 4B. In our erAEQ-transfected cell system, we did not observe any effects of RU360 on $[Ca^{2+}]_{ER}$; therefore, we conclude that RU360 specifically affects $[Ca^{2+}]_{mito}$. Using the Ca^{2+} intake assay, we observed that inhibition of the Ca^{2+} uniporter decreased $[Ca^{2+}]_{mito}$ intake in HT1080/Neo, but had no effect on $[Ca^{2+}]_{mito}$ intake in HT1080/BI-1 (Fig. 4C). We also tested the effects of ER stress in this system and observed that RU360 treatment regulated thapsigargin-induced cell death without affecting the protective effect of overexpression of BI-1 (Fig. 4D). These data suggest that the mitochondrial Ca^{2+} uniporter contributes to mitochondrial Ca^{2+} accumulation upon exposure to ER stress, and that BI-1 regulates the Ca^{2+} uniporter, leading to modulation of mitochondrial Ca^{2+} intake.

BI-1 regulates opening of the mitochondrial membrane permeability transition pore. As a messenger of cell death, mitochondrial Ca^{2+} opens the mitochondrial membrane permeability transition pore (PTP), thereby releasing cytochrome c into the cytoplasm[24]. PTP opening has been shown to be involved in ER stress-associated cell death[25,26]. We therefore examined whether the regulation of PTP is related to the cell protective effect in BI-1–overexpressing cells through trypan blue exclusion analysis. In HT1080/Neo, thapsigargin reduced cell viability to 27%; however, the PTP inhibitor cyclosporine A (CsA) increased cell viability. As expected, HT1080/BI-1 cells were resistant to thapsigargin. The protective effect of BI-1 in HT1080/BI-1 cells was greater than that of CsA in thapsigargin-treated HT1080/Neo cells, implying another protective mechanism in addition to the PTP regulation seen in HT1080/BI-1. The presence of CsA had little effect on the viability of thapsigargin-treated HT1080/BI-1 (Fig. 5A), suggesting that PTP regulation is at least one mechanism by which BI-1 protects cells against thapsigargin. Annexin V/propidium iodide analysis, another assay for cell death, showed similar protection against thapsigargin in HT1080/BI-1 (Fig. 5B). CsA also protected HT1080/Neo against the ER-stress agents, tunicamycin and brefeldin A (Fig. 5C). Consistent with these findings, HT1080/BI-1 cells were protected against the ER-stress agents, and were minimally affected by CsA. To confirm the mechanistic link between Ca^{2+} and the resultant PTP opening, $[Ca^{2+}]_{ER}$ and $[Ca^{2+}]_{mito}$ were analyzed in the presence of ER stress with or without the PTP inhibitor, CsA. CsA treatment did not affect either $[Ca^{2+}]_{ER}$ or $[Ca^{2+}]_{mito}$ in ER stress-exposed HT1080/Neo and HT1080/BI-1 (Fig. 5D), suggesting that PTP opening is not a cause of the Ca^{2+} disturbance, but a consequence of $[Ca^{2+}]_{mito}$ accumulation. For direct PTP measurement, mitochondria from HT1080/Neo and HT1080/BI-1 were exposed to the same amount of Ca^{2+} and mitochondrial swelling was measured. Immunoblotting with anti-Hsp60, anti-caspase-3, or anti-calreticulin antibody confirmed the appropriate mitochondrial fractionation of HT1080/Neo and HT1080/BI-1 (Fig. 6A, upper). To eliminate interference by the small amount of Ca^{2+} released spontaneously from the mitochondria, we routinely included 25 μM EGTA. Under these conditions, mitochondria from HT1080/Neo and HT1080/BI-1 were exogenously exposed to 100 μM Ca^{2+}. Swelling of mitochondria, which is

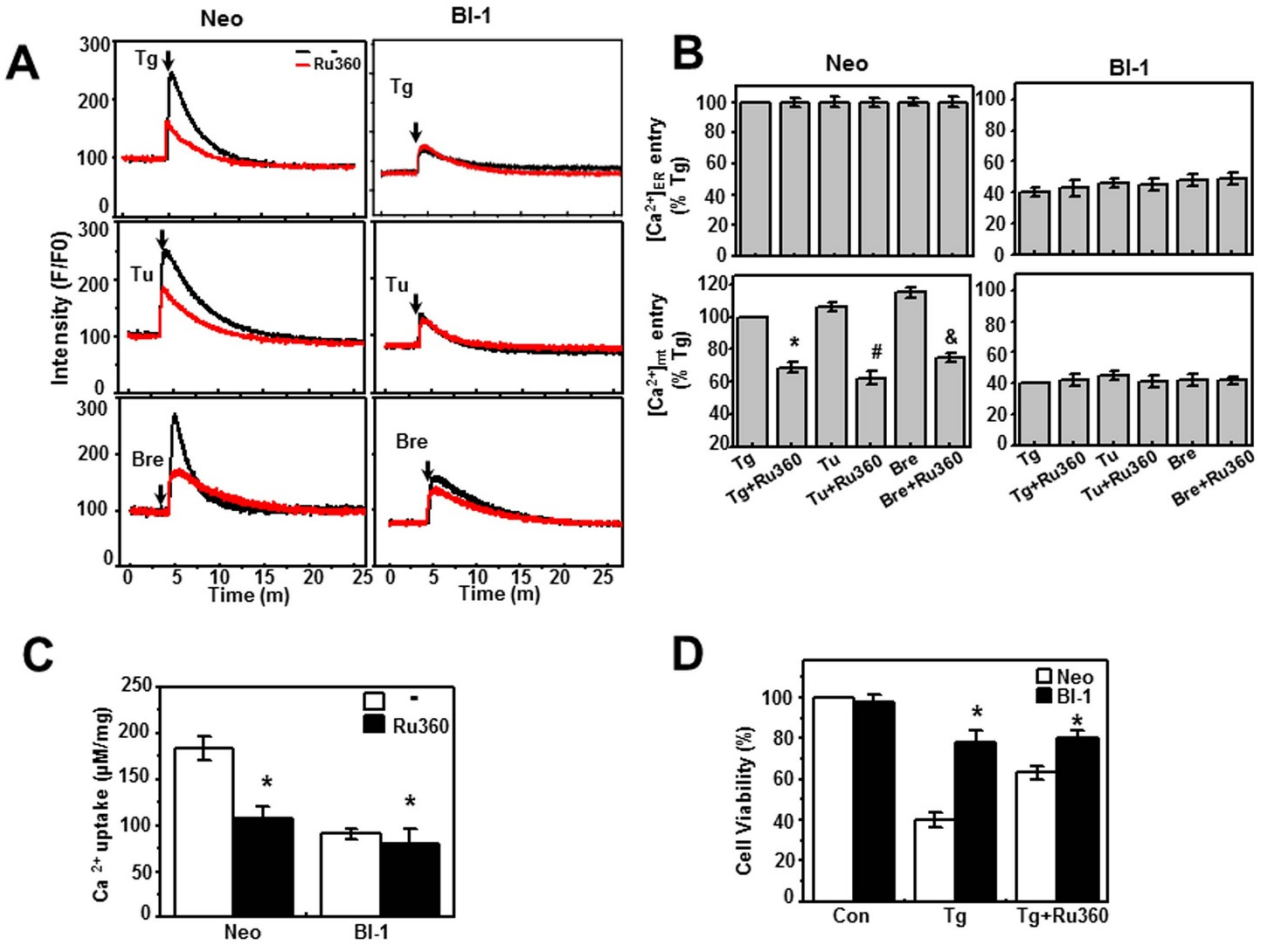

Figure 4 | Mitochondrial Ca^{2+} intake through the Ca^{2+} uniporter is reduced in HT1080/BI-1 cells. (A) HT1080/Neo and HT1080/BI-1 were loaded with Rhod II-AM and subsequently treated with 5 μM thapsigargin, 5 μg/ml tunicamycin, or 1 μM brefeldin A in the presence or absence of 1 μM RU360. Rhod II fluorescence was analyzed. (B) HT1080/Neo and HT1080/BI-1 were transfected with erAEQ or loaded with Rhod II, and treated with 5 μM thapsigargin, 5 μg/ml tunicamycin, or 1 μg/ml brefeldin A in the presence or absence of 1 μM RU360. The intensity of erAEQ luminescence or Rhod II fluorescence was quantified. *, $p < 0.05$ versus thapsigargin-treated HT1080/Neo; #, $p < 0.05$ versus tunicamycin-treated HT1080/Neo; &, $p < 0.05$ versus brefeldin A-treated HT1080/Neo. (C) Mitochondrial $^{45}Ca^{2+}$ intake was analyzed in HT1080/Neo and HT1080/BI-1 in the presence or absence of RU360. *, $p < 0.05$ versus HT1080/Neo without RU360. (D) Viability of HT1080/Neo and HT1080/BI-1 cells after treatment with 5 μM thapsigargin in the presence or absence of RU360 was determined by trypan blue staining. *, $p < 0.05$ versus thapsigargin-treated HT1080/Neo Tg, thapsigargin; Tu, tunicamycin; Bre, brefeldin; Con, Control; Neo, neomycin-resistant pcDNA3-transfected HT1080 cells (HT1080/Neo); BI-1, HA-BI-1-pcDNA3-transfected HT1080 cells (HT1080/BI-1).

considered a marker for PTP opening[27,28], was clearly observed in the Ca^{2+}-exposed mitochondria from HT1080/Neo by monitoring optical density at 540 nm (Fig. 6A). Mitochondrial PTP opening was significantly suppressed by CsA. PTP opening/mitochondria swelling was also observed in Ca^{2+}-exposed mitochondria from HT1080/BI-1, but to a lesser extent than in HT1080/Neo. In the BI-1-overexpression system, treatment with CsA had no additional regulatory effect on PTP opening, suggesting that the presence of BI-1 itself induces the regulation of PTP opening. Accumulation of Ca^{2+} in the mitochondrial matrix induces mitochondrial PTP opening and loss of mitochondrial membrane potential, $\Delta\psi m$[26]. This study also showed a clear loss of $\Delta\psi m$ after Ca^{2+} exposure in HT1080/Neo compared with HT1080/BI-1 (Fig. 6B). The consequential release of cytochrome c was confirmed with purified mitochondria from HT1080/Neo and HT1080/BI-1. Exposure of mitochondria to Ca^{2+} increased the amount of extra-mitochondrial/supernatant cytochrome in the HT1080/Neo group, but this was suppressed by inhibition of PTP opening by CsA (Fig. 6C). However, the release of cytochorome c was not observed in Ca^{2+}-exposed mitochondria from HT1080/BI-1. We next investigated the effects of Ca^{2+} on the induction of cytochrome c release via PTP opening in BI-$1^{+/+}$ and BI-$1^{-/-}$ MEF cells. Immunoblotting with antibodies against Hsp60, caspase-3, or calreticulin confirmed appropriate mitochondrial fractionation from these MEF cells (Fig. 6D, upper). Ca^{2+}-induced PTP opening was greater in BI-$1^{-/-}$ MEF cells; however, CsA was able to effectively block PTP opening in both cell types (Fig. 6D). Although the initial $\Delta\psi m$ was similar between BI-$1^{+/+}$ and BI-$1^{-/-}$ cells, the BI-$1^{-/-}$ cells were more susceptible to Ca^{2+}-induced disruption of $\Delta\psi m$ than BI-$1^{+/+}$ cells (Fig. 6E). Consistent with these findings, cytochrome c release into the extra-mitochondrial environment was higher in BI-$1^{-/-}$ cells than in BI-$1^{+/+}$ cells (Fig. 6F). Mitochondria from BI-$1^{-/-}$ livers also showed higher sensitivity to Ca^{2+}-induced PTP opening and cytochrome c release than mitochondria from BI-$1^{+/+}$ livers (Fig. S1A, B).

The mitochondrial Ca^{2+}-dependent K^+ channel ($mitoK_{Ca}$) is activated in HT1080/BI-1. Under continuous leakage of Ca^{2+} from the ER, other ions such as K^+ enter the mitochondria instead of Ca^{2+} to maintain mitochondrial homeostasis[29,30]. K^+-related channel opening is also involved in the maintenance of mitochondrial membrane potential[31,32]. To understand the role of channel proteins in the $\Delta\psi m$, Ca^{2+}-exposed mitochondria from HT1080/

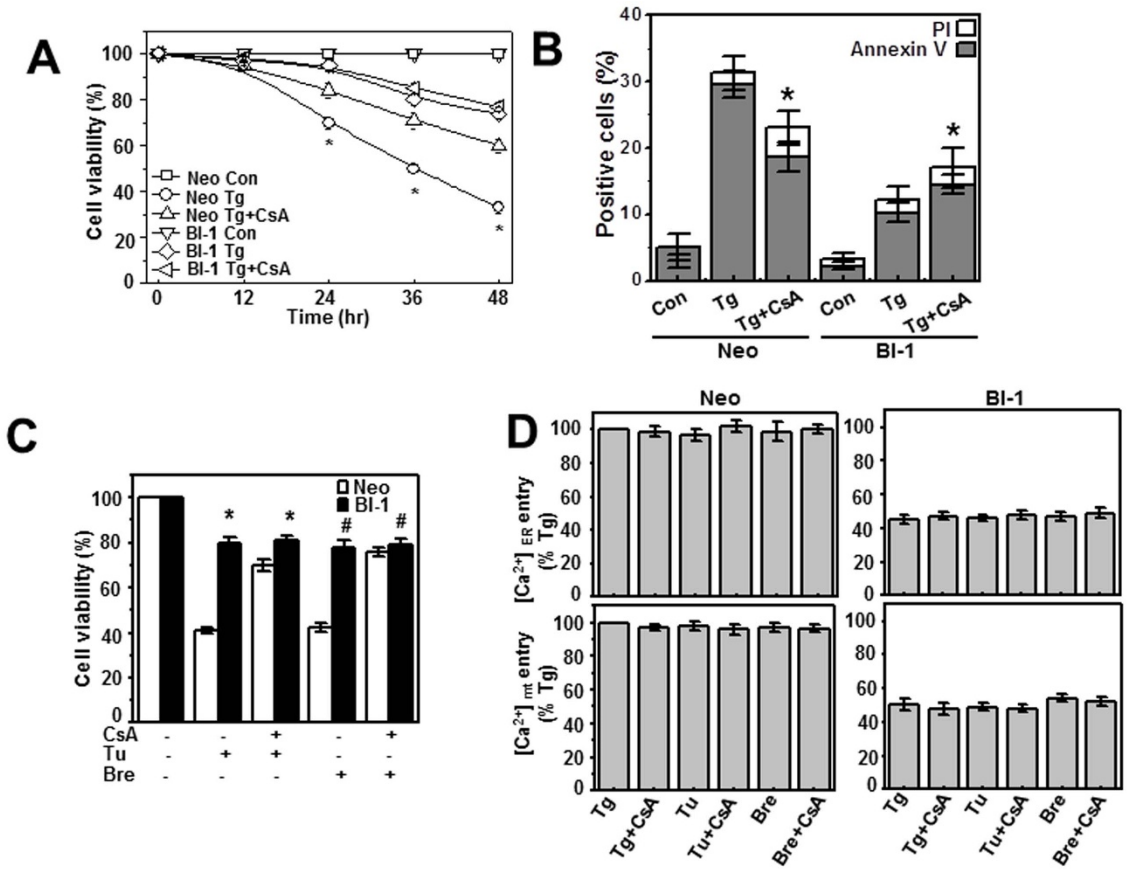

Figure 5 | BI-1 regulates ER stress-induced apoptosis by inhibiting opening of the permeability transition pore. (A) HT1080/Neo and HT1080/BI-1 were treated with thapsigargin in the presence or absence of 5 μM CsA. Cell viability was determined by trypan blue exclusion at 0, 12, 24, 36, and 48 hrs. Data shown represent means ± S.E. (n = 4). (B) HT1080/Neo and HT1080/BI-1 cells were treated with 5 μM thapsigargin in the presence or absence of 5 μM CsA for 24 hrs. Annexin V/PI-stained cells were analyzed by flow cytometry. Data shown represent means ± S.E. (n = 4). *, $p < 0.05$ versus thapsigargin-treated HT1080/Neo. (C) Cell viability was determined by trypan blue exclusion after treatment with 5 μg/ml tunicamycin or 1 μg/ml brefeldin A in the presence or absence of CsA for 48 hrs. *, $p < 0.05$ versus tunicamycin-treated HT1080/Neo; #, $p < 0.05$ versus brefeldin A-treated HT1080/Neo (D) HT1080/Neo and HT1080/BI-1 were transfected with erAEQ or loaded with Rhod II and subsequently treated with either 5 μM thapsigargin, 5 μg/ml tunicamycin, or 1 μg/ml brefeldin A in the presence or absence of 5 μM CsA. After the indicated treatments, the intensity of erAEQ luminescence or Rhod II fluorescence was quantified. Cropped gels/blots were run under the same experimental conditions. CsA, Cyclosporine A; Tg, Thapsigargin; Tu, Tunicamycin; Bre, Brefeldin A; Con, Control; $[Ca^{2+}]_{ER}$ (%TG), Negative peak of luminescence of erAEQ compared to TG; $[Ca^{2+}]_{mito}$ (%TG), peak of fluorescence of Rhod II compared to TG; Neo, neomycin-resistant pcDNA3-transfected HT1080 cells (HT1080/Neo); BI-1, HA-BI-1-pcDNA3-transfected HT1080 cells (HT1080/BI-1).

Neo and HT1080/BI-1 cells were co-treated with NS1619 (a cell-permeable mitoK_{Ca} channel opener[32]), paxilline (a mitoK_{Ca} channel inhibitor[33]), diazoxide (a mitoK_{ATP} channel opener), or 5-hydroxydecanoate (5-HD; a mitoK_{ATP} channel blocker[34]) and the Δψm was measured. Consistent with the data in Fig. 6B, basal Δψm was lower in HT1080/BI-1 than in HT1080/Neo. Under Ca^{2+} exposure, mitochondria from HT1080/BI-1 showed resistance to the Ca^{2+}, revealing a relatively stable Δψm compared with those from HT1080/Neo (Fig. 7A). Among the inhibitors, the mitoK_{Ca} channel inhibitor paxilline had the greatest effect on Δψm in Ca^{2+}-exposed mitochondria from HT1080/BI-1. Compared with HT1080/BI-1, paxilline had less effect on the Δψm in Ca^{2+}-exposed HT1080/Neo, suggesting that BI-1 is involved in opening of the mitochondrial Ca^{2+}-dependent K^+ channel and providing a possible mechanism for the reduced, but stably maintained, Δψm in HT1080/BI-1.

Entry of K^+ through mitochondrial K^+ channels leads to net oxidation of mitochondria. Unique fluorescence assays can measure this oxidation[35,36] and have been used to examine the mitochondrial entry of K^+. Therefore, we performed a flavoprotein fluorescence assay to examine the effects of BI-1 on mitoK_{Ca} channel opening. Figure 7B shows a representative time course of the changes in flavoprotein fluorescence in HT1080/Neo and HT1080/BI-1 cells exposed to NS1619 and/or paxilline. In these experiments, NS1619 reversibly oxidized flavoprotein, with subsequent exposure to 2,4-dinitrophenol (DNP) leading to full flavoprotein oxidation. In the presence of paxilline, NS1619 failed to oxidize flavoprotein, indicating complete inhibition of NS1619-induced oxidation by paxilline. In general, flavoprotein oxidation was higher in HT1080/BI-1 than in HT1080/Neo. We also examined the modulation of mitoK_{Ca} channels in ER stress-exposed cells by examining the effects of thapsigargin on flavoprotein oxidation. Figure 7C shows a representative experiment investigating the effects of thapsigargin on NS1619-induced flavoprotein oxidation. Thapsigargin enhanced the oxidative effect of NS1619, when added after the NS1619 effect had reached a steady state. The thapsigargin-induced flavoprotein oxidation was significantly higher in HT1080/BI-1 than in HT1080/Neo. These results also indicate that mitoK_{Ca} channels are more highly activated in HT1080/BI-1 than in HT1080/Neo.

Analysis of mitochondrial Ca^{2+} revealed that NS1619 treatment markedly inhibited thapsigargin-increased mitochondrial Ca^{2+} concentrations in HT1080/Neo, but only slightly affected mitochondrial

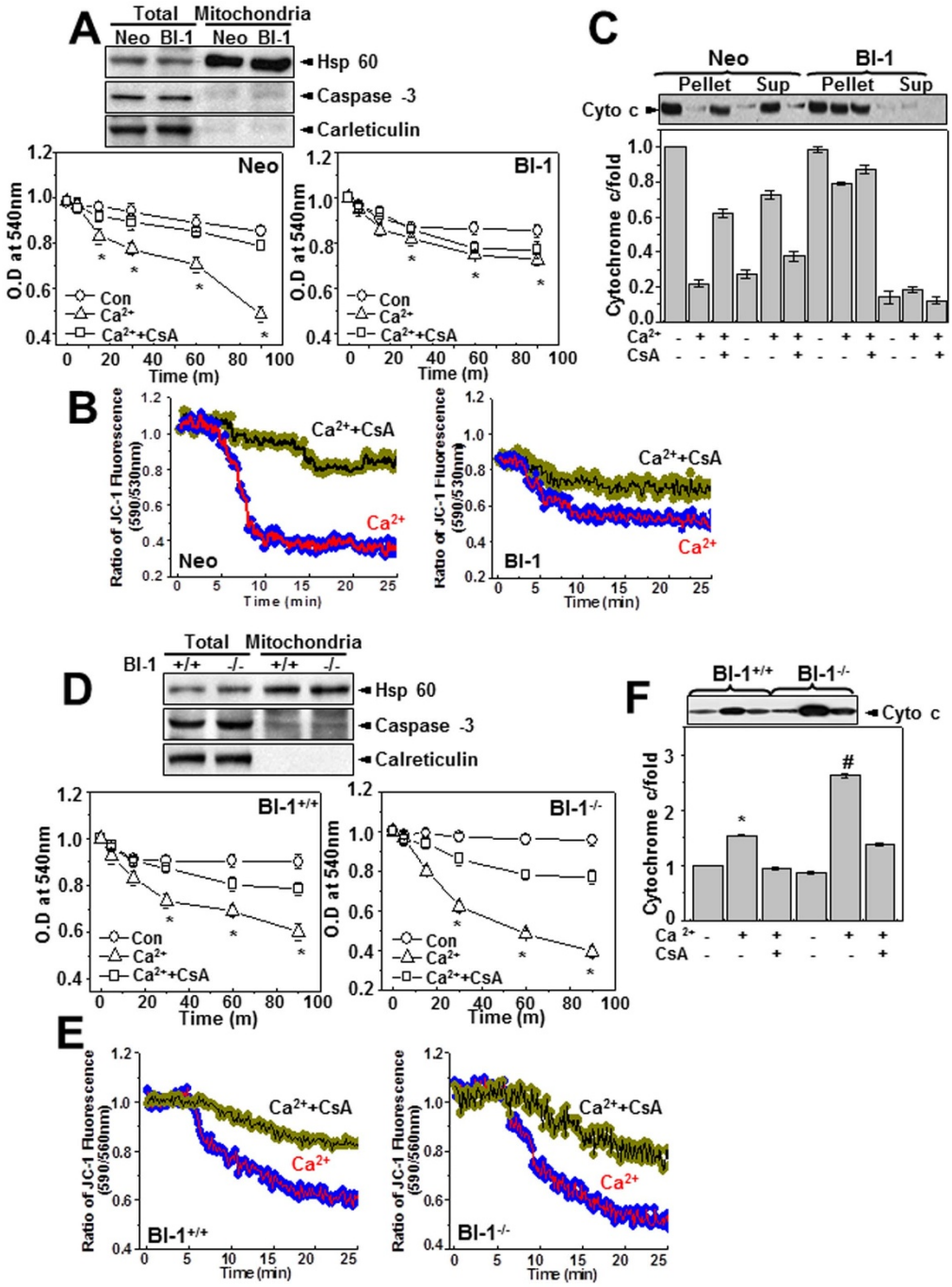

Figure 6 | Ca^{2+}-induced mitochondrial permeability transition pore opening and cytochrome c release are regulated by BI-1. (A) Immunoblotting of total cells and mitochondria fractions from HT1080/Neo and HT1080/BI-1 with anti-Hsp60, anti-caspase-3, or anti-calreticulin antibodies. Mitochondria from HT1080/Neo and HT1080/BI-1 were treated with buffer and 100 μM $CaCl_2$ in the presence or absence of 5 μM CsA. Absorbance at 540 nm was measured at the indicated time points after incubation at 30°C. Data shown are mean ± S.E. (n = 4). *$p < 0.05$ versus Ca^{2+}-exposed mitochondria from HT1080/Neo. (B) Mitochondria from HT1080/Neo and HT1080/BI-1 were loaded with JC-1 dye and treated with 100 μM $CaCl_2$ in the presence or absence of 5 μM CsA. Mitochondrial membrane potential (Δψm) was assessed using a spectrofluorometer as described in the Materials and Methods. (C) Mitochondria from HT1080/Neo and HT1080/BI-1 were treated with 100 μM $CaCl_2$ in the presence or absence of 5 μM CsA. Cytochrome c released into supernatants was detected by immunoblotting with antibody against cytochrome c. Quantification is shown in the bottom panel. (D) Immunoblotting of total cells and mitochondria fractions from BI-$1^{+/+}$ and BI-$1^{-/-}$ MEF with anti-Hsp60, anti-caspase-3, or anti-calreticulin antibodies. Mitochondria from BI-$1^{+/+}$ and BI-$1^{-/-}$ MEF cells were treated with buffer, 100 μM $CaCl_2$, or 100 μM $CaCl_2$ plus 5 μM CsA. Absorbance at 540 nm was measured at the designated time points after incubation at 30°C. *, $p < 0.05$ versus Ca^{2+}-exposed mitochondria from BI-$1^{+/+}$ MEF cells, #, $p < 0.01$ versus Ca^{2+}-exposed mitochondria from BI-$1^{-/-}$ MEF cells. (E) Mitochondria were loaded with JC-1 dye. Δψm was assessed using a spectrofluorimeter as described in the Materials and Methods. (F) Mitochondria were treated with 100 μM $CaCl_2$ in the presence or absence of CsA. Cytochrome c released into the supernatant was detected by immunoblotting with antibody against cytochrome c. Quantification is shown in the bottom panel. *, $p < 0.05$ versus non-treated mitochondria from BI-$1^{+/+}$ MEF cells, #, $p < 0.01$ versus non-treated mitochondria from BI-$1^{-/-}$ MEF cells. CsA: Cyclosporine A, Neo, neomycin-resistant pcDNA3-transfected HT1080 cells (HT1080/Neo); BI-1, HA-BI-1-pcDNA3-transfected HT1080 cells (HT1080/BI-1); BI-$1^{+/+}$, BI-1 wild type mouse embryo fibroblasts; BI-$1^{-/-}$, BI-1 knock-out mouse embryo fibroblasts. Sup, supernatants.

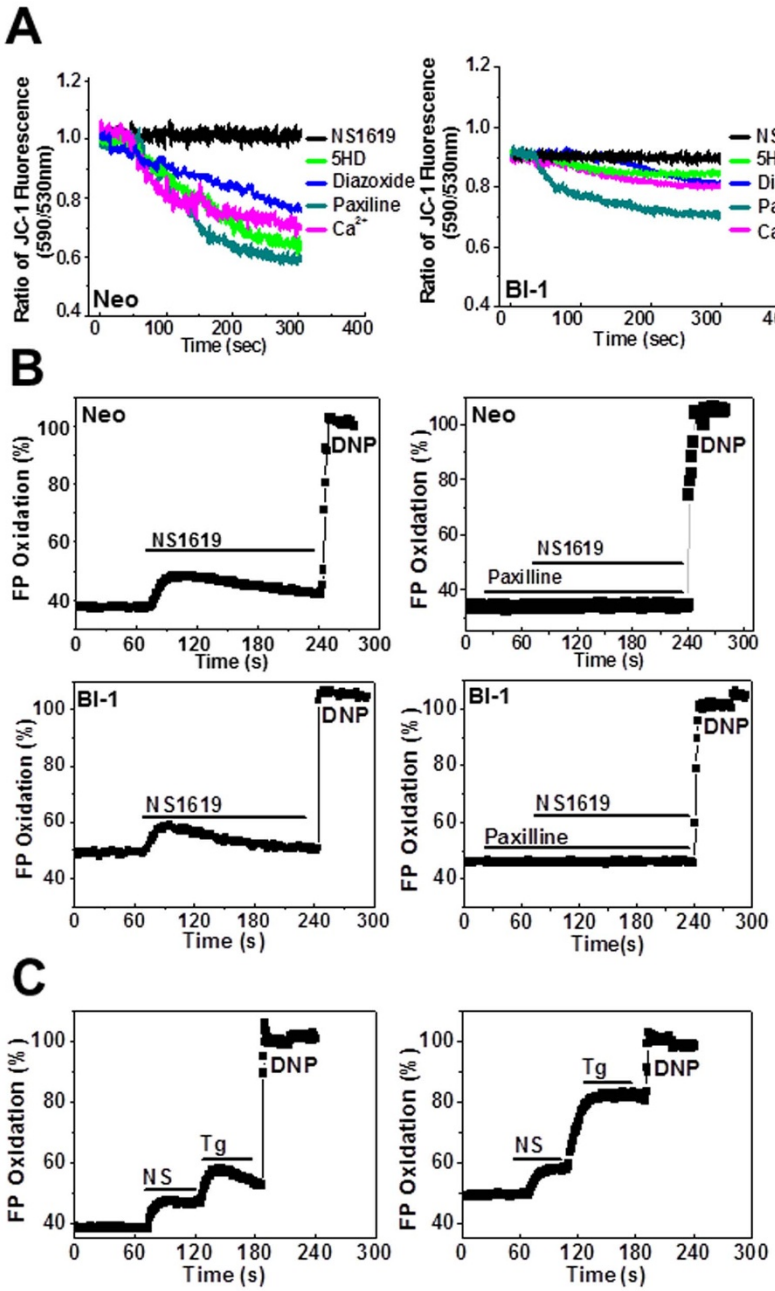

Figure 7 | Activation of the mitochondrial Ca^{2+}-dependent K^+ channel in HT1080/BI-1. (A) Mitochondria isolated from HT1080/Neo and HT1080/BI-1 were exposed to 100 μM Ca^{2+} with or without 100 μM diazoxide, 500 μM 5-HD, 100 μM NS1619, or 2 μM paxilline. Δψm was examined at the indicated times. (B) HT1080/Neo and HT1080/BI-1 were treated with 100 μM NS1619 in the presence or absence of paxilline; flavoprotein fluorescence was calibrated by exposing cells to 100 μmol/L DNP. (C) HT1080/Neo and HT1080/BI-1 were treated with 100 μM NS1619 and subsequently with 5 μM thapsigargin; flavoprotein fluorescence was calibrated by exposing cells to 100 μmol/L DNP. CsA, Cyclosporine; DNP, 2,4-dinitrophenol; Neo, neomycin-resistant pcDNA3-transfected HT1080 cells (HT1080/Neo); BI-1, HA-BI-1-pcDNA3-transfected HT1080 cells (HT1080/BI-1).

Ca^{2+} in HT1080/BI-1 (Fig. 8A). The area under the curve of mitochondrial Ca^{2+} fluorescence was quantified in Figure 8B, and also showed the regulatory effect of NS1619 on mitochondrial Ca^{2+} in HT1080/Neo, but not in HT1080/BI-1. These data suggest that BI-1 is probably involved in the open state of the Ca^{2+}-dependent K^+ channel, leading to the reduced mitochondrial Ca^{2+}. Next, cell viability assays were performed with K^+-modulating agents. No significant effect on the viability of HT1080/Neo or HT1080/BI-1 was seen with either the mitoK_{ATP} channel activator diazoxide or the mitoK_{ATP} channel inhibitor 5-HD. However, the mitoK_{Ca} activator NS1619 significantly protected against thapsigargin or tunicamycin-induced cell death, especially in HT1080/Neo (Fig. 8C, D). Furthermore, the mitoK_{Ca} inhibitor, paxilline, inhibited the BI-1–mediated protection from ER stress, implying that the mitoK_{Ca} channel is activated and functional in HT1080/BI-1. The BI-1–induced regulation of mitochondrial Ca^{2+} and mitoK_{Ca} channel opening was also confirmed in other cells, including BI-1–overexpressing A549 lung carcinoma cells (A549/BI-1) and tetracycline-inducible BI-1–expressing Hela cells (Fig. S2, S3). Taken together, these data indicate that BI-1 activates mitoK_{Ca} channels, and that this activation is related to low mitochondrial Ca^{2+} and protection against ER stress.

Discussion

Results of this study show that BI-1 protects against ER stress-induced cell death by reducing $[Ca^{2+}]_{mito}$ intake, leading to the regulation of mitochondrial PTP opening and cytochrome c release. This

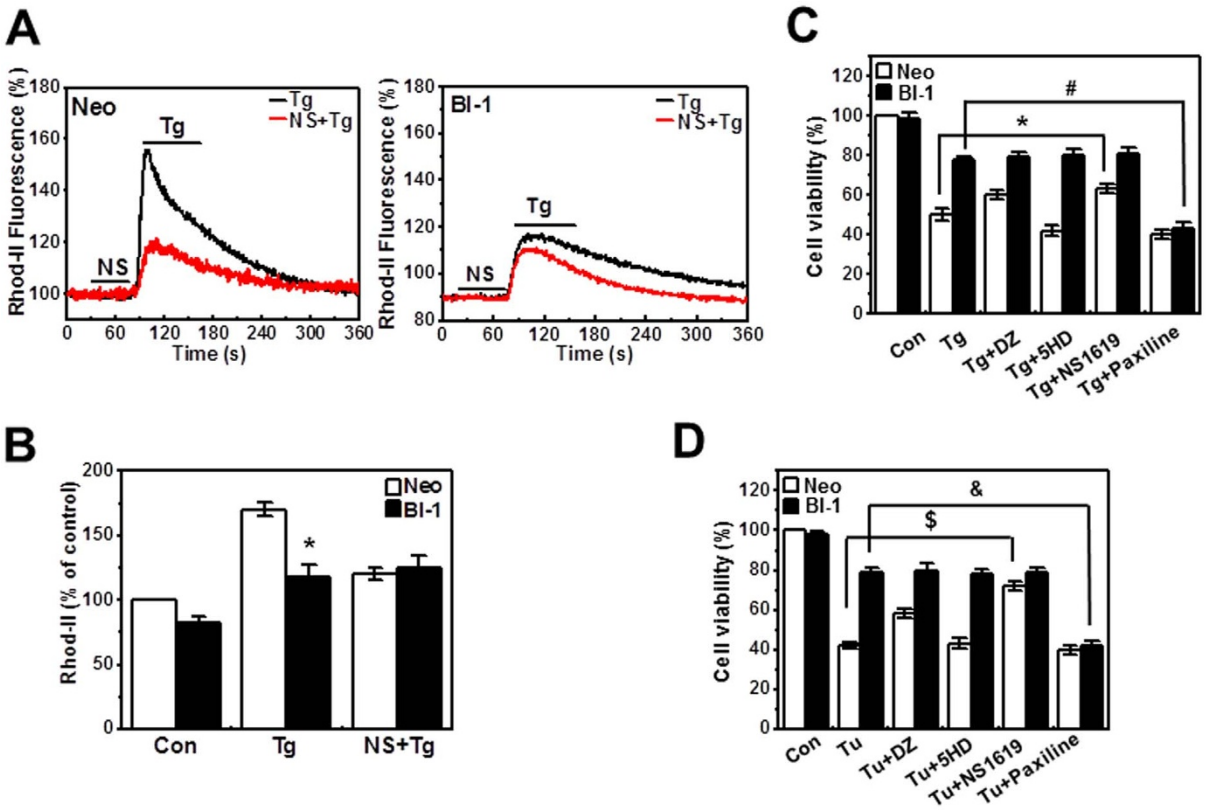

Figure 8 | Mitochondrial Ca^{2+} and cell death are regulated by mitoK_{Ca} channel opening in HT1080/BI-1. (A) HT1080/Neo and HT1080/BI-1 cells were loaded with Rhod II AM and then treated with 5 μM thapsigargin in the presence or absence of NS1619. Rhod II was subsequently monitored. (B) Quantification of Rhod II fluorescence peaks. *, $p < 0.05$ versus thapsigargin-treated HT1080/Neo. HT1080/Neo and HT1080/BI-1 were treated with 5 μM thapsigargin (C) or 5 μg/ml tunicamycin (D) in the presence or absence of 100 μM diazoxide, 500 μM 5-HD, 100 μM NS1619, or 2 μM paxilline for 48 hrs. Cell viability was measured by trypan blue exclusion. *, $p < 0.05$ versus thapsigargin-treated HT1080/Neo; #, $p < 0.05$ versus thapsigargin-treated HT1080/BI-1. $, $p < 0.05$ versus tunicamycin-treated HT1080/Neo; &, $p < 0.05$ versus tunicamycin-treated HT1080/BI-1. 5-HD, 5-hydroxydecanoate; DZ, diazoxide; NS, NS1619; 5HD, 5-hydroxydecanoate; Neo, neomycin-resistant pcDNA3-transfected HT1080 cells (HT1080/Neo); BI-1, HA-BI-1-pcDNA3-transfected HT1080 cells (HT1080/BI-1).

study also suggests that BI-1–associated mitochondrial Ca^{2+} regulation is related to alteration of mitochondrial Ca^{2+} intake capacitance as well as the resistance against ER stress-induced cell death. We propose two mechanisms to explain the reduced amount of mitochondrial Ca^{2+} observed in HT1080/BI-1 cells: (1) ER-localized and MAM-localized BI-1 induces Ca^{2+} leakage from the ER, thereby generating low basal levels of intra-ER Ca^{2+}. Low concentrations of intra-ER Ca^{2+} consequently lead to low concentrations of mitochondrial Ca^{2+} in HT1080/BI-1; (2) Mitochondrial Ca^{2+} intake is altered in HT1080/BI-1. BI-1-mediated regulation of $[Ca^{2+}]_{mito}$ is related to the mitochondrial membrane Ca^{2+} uniporter and mitoK_{Ca} channel opening.

The main theme of this study is why and how mitochondrial Ca^{2+} is maintained at a relatively low level in HT1080/BI-1 cells, compared with HT1080/Neo. When exposed to ER stress, reduced Ca^{2+} transfer from the ER to mitochondria in HT1080/BI-1 could explain the reduced $[Ca^{2+}]_{mito}$ compared with HT1080/Neo (Fig. 2A, B). Even in the absence of stress, HT1080/BI-1 exhibited lower basal $[Ca^{2+}]_{mito}$, probably through ER- or MAM-localized BI-1 Ca^{2+} channel-like activity. The lower $[Ca^{2+}]_{mito}$ in HT1080/BI-1 seems to be related to Ca^{2+} transfer between the ER, with low levels of Ca^{2+}, and the physically juxtaposed mitochondria. However, mitochondria that are not associated with the ER have different mitochondrial Ca^{2+} intake capacitance in HT1080/BI-1 from those in HT1080/Neo (Fig. 3C, 3D). In addition to Ca^{2+} transfer from the ER to physically close mitochondria, the Ca^{2+} intake characteristics of mitochondria may also explain the reduced mitochondrial Ca^{2+} in HT1080/BI-1. To understand this issue, we studied differences in physiological mitochondria functions including mitochondrial membrane potential ($\Delta\psi m$). The basal $\Delta\psi m$, a mitochondrial characteristic used to reflect the Ca^{2+} intake capacity[5,30], was lower in HT1080/BI-1 than in HT1080/Neo (Fig. S4). This observation provides insight into the mechanism of reduced mitochondrial Ca^{2+} intake in HT1080/BI-1 since mitochondrial Ca^{2+} intake depends on $\Delta\psi m$[15]. The opening of the Ca^{2+} uniporter is also dependent upon the $\Delta\psi m$[15]. In HT1080/BI-1, the reduced $\Delta\psi m$ may be one of the mechanisms responsible for reduced Ca^{2+} intake, likely due to reduced Ca^{2+} uniporter activity (Fig. 4A, B).

Based on the reduced mitochondrial Ca^{2+} intake capacitance, we hypothesized that opening of the mitochondrial permeability transition pore associated with mitochondrial Ca^{2+} overload might be attenuated in HT1080/BI-1. For clarification of mitochondrial functional differences between HT1080/Neo and HT1080/BI-1, mitochondria were prepared from both cell lines and exposed to Ca^{2+}. The Ca^{2+}-induced permeability transition pore opening and related cytochrome c release were delayed or inhibited in the presence of BI-1 (Fig. 6A, C, D, F). Even in the absence of ER membrane-localized BI-1, mitochondria membranes from HT1080/BI-1 showed resistance against the loaded Ca^{2+}, suggesting that mitochondrial characteristics might be changed as a result of MAM-localized BI-1. Recently, Sano et al reported a role for BI-1 as a regulator of Ca^{2+} transfer from the ER to mitochondria, thereby changing mitochondrial bioenergetics[37]. We have also reported that BI-1 modulates ATP levels, lactate production, and mitochondrial O_2 consumption[18]. It

has been suggested that the continuous Ca^{2+} leak contributes to the opening of Ca^{2+}-dependent K^+ channels[32]. Due to the K^+ channel opening, aquaporin channel gets to be opened, thereby the intake of water is increased, resulting in swelling of mitochondria[14,38]. In the HT1080/BI-1, the mitochondrial swelling has been also reported[18]. The continuous Ca^{2+} leak might also affect mitochondrial physiological characteristics including electron transfer activity, mitochondrial membrane lipid composition, or mitochondrial membrane potential[39–42]. In HT1080/BI-1, numerous mitochondrial enzymes such as pyruvate dehydrogenase, α-ketoglutarate dehydrogenase, and enzymes for oxidative phosphorylation may be affected by the reduced mitochondrial Ca^{2+} [43]. Similarly, lipid synthesis/metabolism enzymes on the MAM might be affected[44]. In addition, MAM-localized lipid handling has a profound impact on mitochondrial metabolism such as respiration and membrane dynamics[45,46]. These changes in mitochondrial function may affect Ca^{2+} homeostasis in mitochondria, leading to the resistance against Ca^{2+}.

Mitochondrial membrane potential, another factor that is affected by the leakage of Ca^{2+}, was resistant to Ca^{2+} and stably maintained in HT1080/BI-1, compared with HT1080/Neo (Fig. 6A, B). To understand how $\Delta\psi m$ is regulated in the BI-1 system, mitochondrial K^+ channel inhibitors were applied to the Ca^{2+}-induced $\Delta\psi m$ collapse model. The mitoK_{Ca} channel inhibitor paxilline induced the greatest collapse of the stably maintained membrane potential against Ca^{2+} in the BI-1 system (Fig. 7A), indicating that mitoK_{Ca} channel activity contributes to the BI-1-associated stably maintained $\Delta\psi m$. Similarly, $\Delta\psi m$ was previously reported to be regulated by Ca^{2+}-dependent mitochondrial K^+ channel opening/closing[47,48]. Instead of Ca^{2+} continuously entering the mitochondria, cationic ions such as K^+ tend to enter, affecting $\Delta\psi m$[32,48]. It has been suggested that the highly activated K^+ channel is a protective mechanism against ischemia/hypoxic stress-induced intracellular Ca^{2+} overloading[49–51]. Activation of other K^+ channels also contributes to the stably maintained and resistant $\Delta\psi m$ against cell-death stimuli[52,53].

We propose that regulation of mitochondrial Ca^{2+} could explain the protective role of BI-1 against ER stress-induced cell death. Additionally, reactive oxygen species (ROS) are affected by BI-1 and may also contribute to the BI-1 protective mechanism. Both ER stress-mediated production of ROS and subsequent cell death are regulated in BI-1-overexpressing cells[10]. We previously reported that basal ROS levels were significantly lower in HT1080/BI-1 than in HT1080/Neo[10]. Mitochondria are well established as a primary source of ROS[54,55]; activation of the mitochondrial electron transport chain (ETC) leads to electron uncoupling, thereby producing toxic ROS[56]. Since ETC protein complexes are involved in pumping protons (H^+) into the intermembrane space, thereby generating $\Delta\psi m$, the reduced $\Delta\psi m$ observed in HT1080/BI-1 may be linked to reduced ETC activity and the resultant reduction in mitochondrial ROS. We recently observed that mitochondrial ETC activity, in addition to other mitochondrial functions, was stably reduced in HT1080/BI-1, compared with control cells (data not shown). To fully understand the relationship between ROS and BI-1, further experiments are required.

In previous studies on BI-1, Ca^{2+} regulation has been consistently suggested as a protective mechanism against ER stress[8,57,58] The intra-ER leaky Ca^{2+} channel effect seems to be linked to the change in mitochondrial membrane potential and its associated mitochondrial Ca^{2+} intake alteration, as well as the recently reported enhanced lysosomal functional effect[59].

In summary, reduced mitochondrial Ca^{2+} intake is linked to the control of mitochondrial PTP opening and cell death. Our data support a model in which the mitochondrial Ca^{2+} uniporter and the mitoK_{Ca} channel are involved in maintaining low $[Ca^{2+}]_{mito}$ in BI-1-overexpressing cells as part of the mechanism by which BI-1 protects cells from ER stress.

Methods

Materials and cell culture. Unless otherwise noted, reagents, including thapsigargin, tunicamycin, brefeldin A, KCN, and CsA were obtained from Sigma Chemical Company (St. Louis, MO, USA). RU360 was obtained from Calbiochem (San Diego, CA, USA). Fluorescent probes, including Fura2-AM and Rhod II AM, were obtained from Molecular Probes (Eugene, OR, USA). The human HT1080 fibrosarcoma cells were cultured in Dulbecco's modified Eagle's Medium (DMEM) supplemented with 10% fetal bovine serum (FBS), 20 mM Hepes, 100 μg/ml streptomycin, and 100 units/ml penicillin. HT1080 cells were stably transfected with the pcDNA3 (Neo), or pcDNA3-BI-1-HA plasmids using the SuperFect transfection reagent (Qiagen, Valencia, CA). The transfected cells were cultured for 3 weeks in 1 mg/ml G418 (Invitrogen, Carlsbad, CA). Cells were maintained in DMEM containing 10% fetal bovine serum, 1 mM L-glutamine, and penicillin (Invitrogen). The stably transfected cells were named as HT1080/Neo or HT1080/BI-1. Mouse embryonic fibroblasts (MEFs) obtained from BI-$1^{+/+}$ and BI-$1^{-/-}$ mice were cultured in DMEM supplemented as above.

Subcellular fractionation. Cells were resuspended in buffer A [250 mM sucrose, 20 mM HEPES (pH 7.5), 10 mM KCl, 1.5 mM $MgCl_2$, 1 mM EDTA, 1 mM EGTA, and 1× protease inhibitor cocktail] on ice for 30 min prior to lysis with a Dounce homogenizer. Samples were centrifuged at 750 × *g* for 10 min at 4°C to remove unlysed cells and nuclei and the resultant supernatants were centrifuged at 10,000 × *g* for 20 min at 4°C. The pellets (heavy membrane fraction, HM) were used for mitochondrial Ca^{2+} intake experiments, mitochondrial PTP opening assays, and immunoblotting analysis with anti-Hsp60, anti-caspase-3, or anti-cytochrome c antibodies. The supernatants were centrifuged at 100,000 × *g* for 1 hr at 4°C and subsequently loaded onto a three-layered sucrose gradient. Purified ER membranes were then isolated by centrifugation at 152,000 × g. Further purification of mitochondria and the MAM fraction was performed by centrifugation (9,500 × g, 30 min, 4°C) on a 30% Percoll gradient as reported previously[19]. Mitochondria, MAM, and ER fractions were lysed in RIPA buffer (1% sodium deoxycholate, 0.1% SDS, 1% Triton X-100, 10 mM Tris (pH 8.0), 0.14 M NaCl) for immunoblotting with antibodies against calnexin, Tom20, VDAC, HA, or BI-1.

Immunogold electron microscopy. Immunogold experiments were carried out using a previously described method[60,61] with modifications. HT1080 cells were fixed by immersion in Karnovsky solution (2% glutaraldehyde and 2% formaldehyde in 0.05 M sodium cacodylate buffer, pH 7.2) for 4 hrs at 4°C. Cells were then dehydrated in a graded series of ethanol and embedded in Spurr's resin. Thin sections (approximately 80 nm thick) were cut for transmission electron microscopy with a NOVA ultramicrotome (LKB) and picked up on 100-mesh gold grids (Electron Microscopy Sciences). Sections on grids were blocked for 1 hr by floating on drops of PBS containing 3% BSA and 0.05% Triton X-100 (T-PBS), followed by washing on drops of T-PBS (five changes, 3 min each). Sections were then incubated for 4 hrs at 4°C with anti-rat HA (Roche, Mannheim, Germany), or anti-mouse HA antibody (Santa Cruz Biotechnology, Santa Cruz, CA, USA) diluted 1 : 100 in T-PBS containing 0.1% BSA and 0.05% Triton X-100. The grids were washed by floating on drops of T-PBS. Bound antibodies were visualized by incubating the sections with gold-conjugated secondary antibodies (10-nm particle size; Sigma-Aldrich) diluted 1 : 200 in PBS containing 0.1% BSA and 0.05% Triton X-100 for 1 hr. Finally, grids were washed on drops of water (five changes, 5 min each) before being stained with 2% aqueous uranyl acetate for 30 sec. All incubations, except for the primary antibody step, were carried out at room temperature, and all buffers used were 0.22-mm filtrates. The specimens were observed with a transmission electron microscope (H7650, accelerating voltage 100 kV, Hitachi) at the Center for University-Wide Research Facilities (CBNU).

Immunofluorescence microscopy. Immunofluorescence microscopy images were prepared as previously described[62]. HT1080/BI-1 cells were grown on a coverglass bottom dish for 24 hrs. Cells were washed with PBS and fixed with methanol for 5 min. Cells were then incubated overnight with the first primary antibody (1 : 100 dilution; rat anti-HA monoclonal; Roche). The first secondary antibody was FITC-conjugated anti-rat (1 : 200; Invitrogen). After three washes using PBS, cells were incubated with a second primary antibody (1 : 100 dilution for anti-calnexin polyclonal or anti-VDAC polyclonal; Santa Cruz Biotechnology) for 1 hr. The second secondary antibody was TRITC-conjugated anti-rabbit (1 : 200; Invitrogen). Finally, the cells were mounted in VECTASHIELD mounting medium with DAPI. Signals were detected using the FITC, TRITC, and DAPI filter with a Delta Vision Deconvolution Microcopy System (Applied Precision, Issaquah, WA, USA). Colocalization was visualized and Pearson's correlation coefficient of the entire cell was determined using soft image analysis software (Applied Precision).

Measurement of PTP opening and cytochrome c release. Large amplitude swelling was measured as described previously[24] by spectrophotometric measurement of absorbance at 540 nm. Isolated mitochondria (1 mg/ml) were incubated in suspension with various agents in buffer A [200 mM sucrose, 10 mM Tris-MOPS (pH 7.4), 5 mM succinate, 1 mM potassium phosphate, 2 μM rotenone, 1 μg/ml oligomycin, and 25 μM EGTA] at 30°C for 100 min. To monitor mitochondrial swelling, absorbance at A_{540} was measured at designated time points throughout the incubation using a spectrophotometer (Amersham Pharmacia Biotech, Ultrospec Plus). To measure cytochrome c release, 50 μg of mitochondria was incubated at 30°C in 30 μl of Buffer A for 1 hr with various reagents. Supernatants were separated

from mitochondria by centrifugation at 10,000 × *g* for 10 min at 4°C. Supernatants and pellets were resolved by SDS-PAGE on 8-14% gels and immunoblotted with anti-cytochrome c antibodies.

Immunoblotting. Equivalent protein amounts were resolved by SDS-PAGE on 12% acrylamide-0.8% bisacrylamide minigels, electroblotted onto PVDF membranes (Bio-Rad, CA, USA), and sequentially immunoblotted with antibodies against cytochrome c (PharMingen, San Diego, CA, USA), Hsp60 (Stressgen, CA, USA), calreticulin (Santa Cruz Biotechnology), caspase-3 (PharMingen), BI-1 (Abcam, Cambridge, UK) or HA (Roche).

Time-sequential analysis of mitochondrial and ER Ca^{2+} levels. Analysis of mitochondrial Ca^{2+} levels was performed as previously described[11,24]. Briefly, cells were loaded with 1 μM Rhod II AM (Molecular Probes) and 0.02% Pluronic F-127 (Molecular Probes) in Krebs-Ringer bicarbonate buffer [25 mM HEPES (pH 7.2), 111 mM NaCl, 25 mM $NaHCO_3$, 5 mM KCl, 2 mM $CaCl_2$, and 1 mM $MgCl_2$] containing 5 mM glucose for 30 min. Cells were washed once with recording medium containing 129 mM NaCl, 4 mM KCl, 1 mM $MgCl_2$, 2 mM $CaCl_2$, 4.2 mM glucose and 10 mM HEPES (pH 7.4), followed by incubation at room temperature for 60 min in recording medium supplemented with 0.02% Pluronic F-127 and 3 μM Rhod II AM. Culture medium was changed to recording medium, and the cells were exposed to either thapsigargin or tunicamycin. The fluorescence intensity was determined every minute. Images were obtained using a confocal laser-scanning microscope equipped with a helium-neon laser (LSM510, Carl Zeiss, Jena, Germany), using an objective lens with numeral apertures of 0.5 for 20-fold magnification. Fluorescence images labeled with Rhod II were collected using an excitation wavelength of 543 nm. Rhod II fluorescence was detected using single excitation and emission filters and plotted as percentage change from the initial value. Parameters of illumination and detection were controlled digitally for consistent settings throughout the experiments. Two successive digital images were collected, usually at 5126512 pixels in the same visual field. To confirm the dye localization, cells were exposed to Rhod II AM for 1 hr, followed by staining with 100 nM MitoTracker Green FM for 15 min at 37°C. Cells were washed three times and observed under a fluorescence microscope to visualize mitochondria. Drugs were prepared in recording medium immediately before each use.

In separate experiments, measurements of $[Ca^{2+}]_{ER}$ were performed in HT1080/Neo and HT1080/BI-1. Briefly, 24 hrs after transfection with ER-localized aequorin, cells were incubated in saline buffer [135 mM NaCl, 5 mM KCl, 1 mM $MgCl_2$, 1 mM $MgSO_4$, 0.4 mM KH_2PO_4, 5.5 mM glucose and 20 mM 4-(2-hydroxyethyl)-1-piperazineethanesulfonic acid, pH 7.4] supplemented with 5 mM n-coelenterazine, 4 mM ionomycin, and 600 mM ethyleneglycol tetra-acetic acid (EGTA) at 37°C for 40 min. Cells were transferred to a perfusion chamber within a purpose-built luminometer, washed extensively with saline buffer containing 100 mM EGTA and 2% bovine serum albumin, and exposed to thapsigargin. The fluorescence intensity was determined every minute. Light emission was measured in a luminescence counter (MicroBeta, LumiJET Microplate Counter PerkinElmer) at 469 nm every 0.1 sec. Finally, to release the remaining aequorin pool and to calibrate the aequorin signal, the cells were lysed with 100 mM digitonin in a hypotonic Ca^{2+}-rich solution (10 mM $CaCl_2$ in H_2O). Aequorin luminescence signals were collected and calibrated to $[Ca^{2+}]$ values as described previously[63].

Mitochondrial Ca^{2+} analysis using the mitochondrial uncoupler CCCP. To compare mitochondrial Ca^{2+} between HT1080/Neo and HT1080/BI-1, cells were plated onto glass-bottomed perfusion chambers. The chambers were mounted on the stage of an inverted microscope (Nikon Eclipse TE2000) and incubated with Fura-2 AM (2 μM, 1-[2-(5-carboxyoxazol-2-yl)-6-aminobenzoFURAn-5-oxy]-2-(2-amino-5-methylphenoxy)-ethane-*N,N,N′N′*-tetraacetic acid pentaacetoxymethyl ester, Molecular Probes) for 30 min at room temperature in Hanks' balanced salt solution (HBSS). After loading, cells were washed three times in isotonic buffer without Ca^{2+} (KH buffer: 132 mM NaCl, 5 mM KCl, 10 mM dextrose, 10 mM HEPES, 1.05 mM $MgCl_2$). Cells were then promptly treated with 1 μM CCCP (Carbonyl cyanide *m*-chlorophenyl hydrazone), a mitochondrial uncoupler, to compare the amount of mitochondrial Ca^{2+} between HT1080/Neo and HT1080/BI-1[64]. As an indirect marker for $[Ca^{2+}]_{mt}$, changes in $[Ca^{2+}]_i$ as a result of treatment with CCCP were determined as a ratio of 340 nm/380 nm excitation for 512 nm emission using an integrated spectrofluorometer (Photon Technology International, Birmingham, NJ). Ca^{2+} concentrations were calculated using the equation $[Ca^{2+}]_i = K_d\,(F_{380}\mathrm{max}/F_{380}\mathrm{min})\,(R - R_{\mathrm{min}})/(R_{\mathrm{max}} - R)$; a K_d value of 229 nM was assumed for the binding of calcium to Fura-2AM. R_{max} and R_{min} were determined in each experimental group by the consecutive addition of 30 μM digitonin (R_{max}) and 50 mM EGTA (R_{min}). Using CCCP, mitochondrial Ca^{2+} was also measured in a Rhod II AM dye-loaded condition, similar to the time-sequential analysis of mitochondrial Ca^{2+} described above.

Mitochondrial Ca^{2+} intake analysis. Mitochondrial Ca^{2+} intake was measured using $^{45}Ca^{2+}$. Mitochondria vesicles were suspended (1 mg/mL final concentration) in a buffer solution containing 100 mM KCl and 20 mM MOPS-Tris (pH 7.2). Free Ca^{2+} concentration in the incubation buffer was fixed at the desired values using different amounts of $CaCl_2$ (containing 1 μCi $^{45}Ca^{2+}$ $mmol^{-1}$ $CaCl_2$, Amersham, Buckinghamshire, UK) and EGTA. Vesicles were incubated in the buffer at 25°C for 1 min and transport was initiated at time zero. Ca^{2+} intake buffer (129 mM NaCl, 4 mM $MgCl_2$, 0.1 mM $CaCl_2$, 4.2 mM glucose, 2 mM succinate and 10 mM HEPES, pH 7.4) was mixed with 1 μCi $^{45}Ca^{2+}$ and 2 mM ATP at 37°C. The reaction was started by addition of 100 μL of protein (250 μg, total volume 500 μL). At defined time intervals 100-μL aliquots were removed, filtered on pre-wetted nitrocellulose filters (0.45-μm pore size, type WCN, Whatman, Clifton, NJ), and rapidly washed twice with 5 mL of ice-cold wash medium (140 mM KCl, 10 mM NaCl, 2.5 mM $MgCl_2$, 10 mM Hepes-KOH, pH 7.0,). Filtration and rinsing were completed within 30 sec. Samples of 250 μL were placed in a scintillation vial, dissolved in 1 ml scintillation grade 2-methoxyethanol, and counted in a liquid scintillation analyzer (Packard Instruments Co., Downers Grove, IL). All experiments were performed using triplicates, and each experiment was performed at least twice. Separately, mitochondrial Ca^{2+} intake from the medium was measured with Rhod II AM. Briefly, isolated mitochondria (0.5 mg protein) were suspended in 2 mL high KCl buffer (110 mM KCL, 0.5 mM KH_2PO_4, 1 mM $MgCl_2$, 20 mM HEPES, 0.01 mM EGTA, 5 mM succinate at pH 7.2) and fluorescence was recorded at room temperature at 550 nm excitation and 580 emission (Photon Technology International, Birmingham, NJ). F_{min} and F_{max} were established by addition of 1 mM EGTA and 10 mM Ca^{2+}.

JC-1 assay for mitochondrial membrane potential. This assay is based on the changes in electrochemical gradient across the mitochondrial membrane measured by membrane potential ($\Delta\psi m$)[65]. Loss of $\Delta\psi m$ is detected by a fluorescent cationic dye JC-1 (5,59,6,69-tetra chloro-1,19,3,39-tetraethylbenzamidazolo-carbocyanin iodide (Cell Technology, Mountain View, CA). Briefly, freshly isolated mitochondria were labeled with JC-1 for 15 min at 37°C in a 5% CO_2 incubator. After two washes with assay buffer, JC-1 labeled and unlabeled mitochondria suspensions were transferred to 96-well black-walled plates. Fluorescence intensity was read at excitation 550 nm, emission 600 nm for red fluorescence and at excitation 485 nm, emission 535 nm for green fluorescence using a SpectraMax fluorescence plate reader (Molecular Devices, Sunnyvale, CA). The ratio of red to green determined the mitochondria membrane potential. A decrease in the ratio indicated collapse of $\Delta\psi m$.

Assessment of cell death. Cell-surface exposure of phosphatidylserine was assessed by Annexin V/PI fluorescence (MACS, Miltenyi Biotech) according to the manufacturer's protocol. Briefly, 2×10^5 cells were collected, washed in PBS, pelleted, and resuspended in incubation buffer [10 mM HEPES/NaOH (pH 7.4), 140 mM NaCl, and 5 mM $CaCl_2$] containing 1% Annexin V. Samples were incubated in the dark for 15 min prior to addition of another 400 μl of incubation buffer, and subsequently analyzed with a fluorescence-activated cell sorter (Partec, Germany). To measure cell viability, a trypan blue exclusion assay was performed as described previously[66]. Briefly, treated or non-treated cells were assessed microscopically for dead cells by trypan blue exclusion. Cell viability was calculated by dividing the non-stained (viable) cell count by the total cell count. The number of cells was determined by averaging the number of cells in four squares and multiplying this average by a dilution factor.

Flavoprotein fluorescence. Autofluorescence of mitochondrial flavoprotein was measured using a modified version of a previously reported method[11,48]. Briefly, cells were superfused with glucose-free Tyrode's solution containing 140 mmol/L NaCl, 5.4 mmol/L KCl, 1.8 mmol/L $CaCl_2$, 0.33 mmol/L NaH_2PO_4, 0.5 mmol/L $MgCl_2$, and 5 mmol/L HEPES (pH 7.4) at room temperature (22°C). Flavoprotein fluorescence was measured with excitation at 480 nm and emission at 520 nm. Relative fluorescence was calibrated according to signals after application of the mitochondrial uncoupler 2,4-dinitrophenol (DNP) (100 μmol/L).

Statistical analysis. Results are presented as means ± S.E. of n cells. Paired and unpaired Student's *t*-tests were used to determine statistically significant differences between test and control conditions as appropriate. MicroCal Origin software (Northampton, MA, USA) was used for statistical calculations.

1. Berridge, M. J. The endoplasmic reticulum: a multifunctional signaling organelle. *Cell Calcium* **32**, 235–49 (2002).
2. Van Coppenolle, F. *et al.* Ribosome-translocon complex mediates calcium leakage from endoplasmic reticulum stores. *J Cell Sci* **117**, 4135–42 (2004).
3. Pinton, P., Giorgi, C., Siviero, R., Zecchini, E. & Rizzuto, R. Calcium and apoptosis: ER-mitochondria Ca2+ transfer in the control of apoptosis. *Oncogene* **27**, 6407–18 (2008).
4. Giorgi, C. *et al.* Mitochondrial calcium homeostasis as potential target for mitochondrial medicine. *Mitochondrion* **12**, 77–85 (2012).
5. Ben-Hail, D., Palty, R. & Shoshan-Barmatz, V. Measurement of Mitochondrial Ca2+ Transport Mediated by Three Transport Proteins: VDAC1, the Na+/Ca2+ Exchanger, and the Ca2+ Uniporter. *Cold Spring Harb Protoc* **2**, 161–166 (2014).
6. Pinton, P. & Rizzuto, R. Bcl-2 and Ca2+ homeostasis in the endoplasmic reticulum. *Cell Death Differ* **13**, 1409–18 (2006).
7. Zhang, D. & Armstrong, J. S. Bax and the mitochondrial permeability transition cooperate in the release of cytochrome c during endoplasmic reticulum-stress-induced apoptosis. *Cell Death Differ* **14**, 703–15 (2007).
8. Chae, H. J. *et al.* BI-1 regulates an apoptosis pathway linked to endoplasmic reticulum stress. *Mol Cell* **15**, 355–66 (2004).
9. Bailly-Maitre, B. *et al.* Cytoprotective gene bi-1 is required for intrinsic protection from endoplasmic reticulum stress and ischemia-reperfusion injury. *Proc Natl Acad Sci U S A* **103**, 2809–14 (2006).

10. Lee, G. H. *et al.* Bax inhibitor-1 regulates endoplasmic reticulum stress-associated reactive oxygen species and heme oxygenase-1 expression. *J Biol Chem* **282**, 21618–28 (2007).
11. Kim, H. R. *et al.* Bax Inhibitor-1 Is a pH-dependent regulator of Ca2+ channel activity in the endoplasmic reticulum. *J Biol Chem* **283**, 15946–55 (2008).
12. Xu, C., Xu, W., Palmer, A. E. & Reed, J. C. BI-1 regulates endoplasmic reticulum Ca2+ homeostasis downstream of Bcl-2 family proteins. *J Biol Chem* **283**, 11477–84 (2008).
13. Ferreiro, E. *et al.* Involvement of mitochondria in endoplasmic reticulum stress-induced apoptotic cell death pathway triggered by the prion peptide PrP(106-126). *J Neurochem* **104**, 766–76 (2008).
14. Kaasik, A., Safiulina, D., Zharkovsky, A. & Veksler, V. Regulation of mitochondrial matrix volume. *Am J Physiol Cell Physiol* **292**, C157–63 (2007).
15. Rodrigo, G. C. & Standen, N. B. Role of mitochondrial re-energization and Ca2+ influx in reperfusion injury of metabolically inhibited cardiac myocytes. *Cardiovasc Res* **67**, 291–300 (2005).
16. Glab, M., Lojek, A., Wrzosek, A., Dolowy, K. & Szewczyk, A. Endothelial mitochondria as a possible target for potassium channel modulators. *Pharmacol Rep* **58 Suppl**, 89–95 (2006).
17. Oshima, R. *et al.* The Bax lnhibitor-1 needs a functional electron transport chain for cell death suppression. *FEBS Lett* **581**, 4627–32 (2007).
18. Lee, G. H. *et al.* BAX inhibitor-1 enhances cancer metastasis by altering glucose metabolism and activating the sodium-hydrogen exchanger: the alteration of mitochondrial function. *Oncogene* **29**, 2130–41 (2010).
19. Wieckowski, M. R., Giorgi, C., Lebiedzinska, M., Duszynski, J. & Pinton, P. Isolation of mitochondria-associated membranes and mitochondria from animal tissues and cells. *Nat Protoc* **4**, 1582–90 (2009).
20. Hamasaki, M. *et al.* Autophagosomes form at ER-mitochondria contact sites. *Nature* **495**, 389–93 (2013).
21. Bononi, A. *et al.* Identification of PTEN at the ER and MAMs and its regulation of Ca(2+) signaling and apoptosis in a protein phosphatase-dependent manner. *Cell Death Differ* **20**, 1631–43 (2013).
22. Krajewska, M. *et al.* Endoplasmic reticulum protein BI-1 modulates unfolded protein response signaling and protects against stroke and traumatic brain injury. *Brain Res* **1370**, 227–37 (2011).
23. Zhang, Y., Soboloff, J., Zhu, Z. & Berger, S. A. Inhibition of Ca2+ influx is required for mitochondrial reactive oxygen species-induced endoplasmic reticulum Ca2+ depletion and cell death in leukemia cells. *Mol Pharmacol* **70**, 1424–34 (2006).
24. Bernardi, P. & Rasola, A. Calcium and cell death: the mitochondrial connection. *Subcell Biochem* **45**, 481–506 (2007).
25. Deniaud, A. *et al.* Endoplasmic reticulum stress induces calcium-dependent permeability transition, mitochondrial outer membrane permeabilization and apoptosis. *Oncogene* **27**, 285–99 (2008).
26. Colell, A. *et al.* Cholesterol impairs the adenine nucleotide translocator-mediated mitochondrial permeability transition through altered membrane fluidity. *J Biol Chem* **278**, 33928–35 (2003).
27. Park, J. H. & Kim, T. H. Release of cytochrome c from isolated mitochondria by etoposide. *J Biochem Mol Biol* **38**, 619–23 (2005).
28. Kim, T. H., Zhao, Y., Barber, M. J., Kuharsky, D. K. & Yin, X. M. Bid-induced cytochrome c release is mediated by a pathway independent of mitochondrial permeability transition pore and Bax. *J Biol Chem* **275**, 39474–81 (2000).
29. Awede, B., Berquin, A., Wuytack, F. & Lebacq, J. Adaptation of mouse skeletal muscle to a novel functional overload test: changes in myosin heavy chains and SERCA and physiological consequences. *Eur J Appl Physiol Occup Physiol* **80**, 519–26 (1999).
30. Sato, T., O'Rourke, B. & Marban, E. Modulation of mitochondrial ATP-dependent K+ channels by protein kinase C. *Circ Res* **83**, 110–4 (1998).
31. Bednarczyk, P. Potassium channels in brain mitochondria. *Acta Biochim Pol* **56**, 385–92 (2009).
32. Skalska, J. *et al.* Calcium ions regulate K(+) uptake into brain mitochondria: the evidence for a novel potassium channel. *Int J Mol Sci* **10**, 1104–20 (2009).
33. O'Rourke, B. Evidence for mitochondrial K+ channels and their role in cardioprotection. *Circ Res* **94**, 420–32 (2004).
34. Liu, Y., Sato, T., O'Rourke, B. & Marban, E. Mitochondrial ATP-dependent potassium channels: novel effectors of cardioprotection? *Circulation* **97**, 2463–9 (1998).
35. Kohro, S., Hogan, Q. H., Warltier, D. C. & Bosnjak, Z. J. Protein kinase C inhibitors produce mitochondrial flavoprotein oxidation in cardiac myocytes. *Anesth Analg* **99**, 1316–22 (2004).
36. Pasdois, P. *et al.* Effect of diazoxide on flavoprotein oxidation and reactive oxygen species generation during ischemia-reperfusion: a study on Langendorff-perfused rat hearts using optic fibers. *Am J Physiol Heart Circ Physiol* **294**, H2088–97 (2008).
37. Sano, R. *et al.* Endoplasmic reticulum protein BI-1 regulates Ca(2)(+)-mediated bioenergetics to promote autophagy. *Genes Dev* **26**, 1041–54 (2012).
38. Lee, W. K. & Thevenod, F. A role for mitochondrial aquaporins in cellular life-and-death decisions? *Am J Physiol Cell Physiol* **291**, C195–202 (2006).
39. Raturi, A. & Simmen, T. Where the endoplasmic reticulum and the mitochondrion tie the knot: the mitochondria-associated membrane (MAM). *Biochim Biophys Acta* **1833**, 213–24 (2013).
40. Rizzuto, R. *et al.* Ca(2+) transfer from the ER to mitochondria: when, how and why. *Biochim Biophys Acta* **1787**, 1342–51 (2009).
41. Duchen, M. R. Mitochondria and calcium: from cell signalling to cell death. *J Physiol* **529 Pt 1**, 57–68 (2000).
42. Pradhan, R. K., Qi, F., Beard, D. A. & Dash, R. K. Characterization of membrane potential dependency of mitochondrial Ca2+ uptake by an improved biophysical model of mitochondrial Ca2+ uniporter. *PLoS One* **5**, e13278 (2010).
43. Gellerich, F. N. *et al.* The regulation of OXPHOS by extramitochondrial calcium. *Biochim Biophys Acta* **1797**, 1018–27 (2010).
44. Sano, R. *et al.* GM1-ganglioside accumulation at the mitochondria-associated ER membranes links ER stress to Ca(2+)-dependent mitochondrial apoptosis. *Mol Cell* **36**, 500–11 (2009).
45. Birner, R., Burgermeister, M., Schneiter, R. & Daum, G. Roles of phosphatidylethanolamine and of its several biosynthetic pathways in Saccharomyces cerevisiae. *Mol Biol Cell* **12**, 997–1007 (2001).
46. Steenbergen, R. *et al.* Disruption of the phosphatidylserine decarboxylase gene in mice causes embryonic lethality and mitochondrial defects. *J Biol Chem* **280**, 40032–40 (2005).
47. Szewczyk, A., Jarmuszkiewicz, W. & Kunz, W. S. Mitochondrial potassium channels. *IUBMB Life* **61**, 134–43 (2009).
48. Sato, T., Saito, T., Saegusa, N. & Nakaya, H. Mitochondrial Ca2+-activated K+ channels in cardiac myocytes: a mechanism of the cardioprotective effect and modulation by protein kinase A. *Circulation* **111**, 198–203 (2005).
49. Xu, W. *et al.* Cytoprotective role of Ca2+- activated K+ channels in the cardiac inner mitochondrial membrane. *Science* **298**, 1029–33 (2002).
50. Xie, Y. *et al.* Intermittent high altitude hypoxia protects the heart against lethal Ca^{2+} overload injury. *Life Sci* **76**, 559–72 (2004).
51. Borchert, G. H., Yang, C. & Kolar, F. Mitochondrial BKCa channels contribute to protection of cardiomyocytes isolated from chronically hypoxic rats. *Am J Physiol Heart Circ Physiol* **300**, H507–13 (2011).
52. Kullin, M. *et al.* Protection of rat pancreatic islets by potassium channel openers against alloxan, sodium nitroprusside and interleukin-1beta mediated suppression--possible involvement of the mitochondrial membrane potential. *Diabetologia* **46**, 80–8 (2003).
53. Xie, J. *et al.* K(ATP) channel openers protect mesencephalic neurons against MPP+-induced cytotoxicity via inhibition of ROS production. *J Neurosci Res* **88**, 428–37 (2010).
54. Brookes, P. S., Yoon, Y., Robotham, J. L., Anders, M. W. & Sheu, S. S. Calcium, ATP, and ROS: a mitochondrial love-hate triangle. *Am J Physiol Cell Physiol* **287**, C817–33 (2004).
55. Murphy, M. P. How mitochondria produce reactive oxygen species. *Biochem J* **417**, 1–13 (2009).
56. Kowaltowski, A. J., de Souza-Pinto, N. C., Castilho, R. F. & Vercesi, A. E. Mitochondria and reactive oxygen species. *Free Radic Biol Med* **47**, 333–43 (2009).
57. Hunsberger, J. G. *et al.* Bax inhibitor 1, a modulator of calcium homeostasis, confers affective resilience. *Brain Res* **1403**, 19–27 (2011).
58. Ishikawa, T., Watanabe, N., Nagano, M., Kawai-Yamada, M. & Lam, E. Bax inhibitor-1: a highly conserved endoplasmic reticulum-resident cell death suppressor. *Cell Death Differ* **18**, 1271–8 (2011).
59. Lee, G. H. *et al.* Enhanced lysosomal activity is involved in Bax inhibitor-1-induced regulation of the endoplasmic reticulum (ER) stress response and cell death against ER stress: involvement of vacuolar H+-ATPase (V-ATPase). *J Biol Chem* **286**, 24743–53 (2011).
60. Park, K. H. *et al.* Ca2+ signaling tools acquired from prostasomes are required for progesterone-induced sperm motility. *Sci Signal* **4**, ra31 (2011).
61. Giorgi, C. *et al.* PML regulates apoptosis at endoplasmic reticulum by modulating calcium release. *Science* **330**, 1247–51 (2010).
62. Gilady, S. Y. *et al.* Ero1alpha requires oxidizing and normoxic conditions to localize to the mitochondria-associated membrane (MAM). *Cell Stress Chaperones* **15**, 619–29 (2010).
63. Chiesa, A. *et al.* Recombinant aequorin and green fluorescent protein as valuable tools in the study of cell signalling. *Biochem J* **355**, 1–12 (2001).
64. Mallilankaraman, K. *et al.* MCUR1 is an essential component of mitochondrial Ca2+ uptake that regulates cellular metabolism. *Nat Cell Biol* **14**, 1336–43 (2012).
65. Joiner, M. L. *et al.* CaMKII determines mitochondrial stress responses in heart. *Nature* **491**, 269–73 (2012).
66. Shin, Y. J. *et al.* Autophagy induction and CHOP under-expression promotes survival of fibroblasts from rheumatoid arthritis patients under endoplasmic reticulum stress. *Arthritis Res Ther* **12**, R19 (2010).

Acknowledgments

This work was supported by a Korea Science and Engineering Foundation Grant (2012R1A2A1A03001907).

Author contributions

All authors contributed to this work. G.H.L. and H.J.C. conceived and designed the experiments; G.H.L. and B.L. performed the experiments; H.R.K. contributed reagents/materials/analysis tools; G.H.L., H.Y.L. and H.J.C. wrote the paper.

Additional information

Supplementary information accompanies this paper at http://www.nature.com/scientificreports

Competing financial interests: The authors declare no competing financial interests.

How to cite this article: Lee, G.-H., Lee, H.-Y., Li, B., Kim, H.-R. & Chae, H.-J. Bax Inhibitor-1-Mediated Inhibition of Mitochondrial Ca^{2+} Intake Regulates Mitochondrial Permeability Transition Pore Opening and Cell Death. *Sci. Rep.* **4**, 5194; DOI:10.1038/srep05194 (2014).

This work is licensed under a Creative Commons Attribution-NonCommercial-ShareAlike 3.0 Unported License. The images in this article are included in the article's Creative Commons license, unless indicated otherwise in the image credit; if the image is not included under the Creative Commons license, users will need to obtain permission from the license holder in order to reproduce the image. To view a copy of this license, visit http://creativecommons.org/licenses/by-nc-sa/3.0/